WWW.IJRPR.COM

**International Journal of Research Publication and Reviews**

Journal Homepage: www.ijrpr.com ISSN 2582-7421

# High Voltage Power Transmission

***Gaware Akshay Madhukar[1], Kishor Eknath Doke[2]and Dhanshri Shantaram Dhanwate[3]***

*[1-3]Department of Electrical Engineering, NIT's Late Annasaheb Patil Polytechnic, Nashik, Maharashtra, India*
*Email: gawareakshay123@gmail.com , kishordoke162@gmail.com, dhanshridhanwate96@gmail.com*

**ABSTRACT—**

High voltage (HV) transmission carries bulk electric power from generation to load centers with low losses, but the choice of voltage and of AC or DC technology involves technical and economic trade-offs. This paper presents a quantitative study of HV overhead transmission. Line parameters, surge impedance loading (SIL) and thermal ratings are calculated for 220, 400 and 765 kV lines; conductor surface gradients are compared with corona onset; long-line voltage behavior and power-transfer capability are analyzed with shunt and series compensation; loadability is mapped against line length; and HVAC and HVDC are compared on present-value cost. For a fixed 500 MW transfer, raising the voltage from 220 to 765 kV cuts $I^2R$ loss from 3.95% to 0.33% per 100 km. A 300 km 400 kV line shows a 5.3% no-load voltage rise, reduced to 2.6% with 50% shunt compensation, and 40% series compensation raises the power-transfer limit from 584 to 899 MW. Under the stated cost assumptions HVDC becomes cheaper beyond about 740 km, with a range of 515–1040 km across converter cost and energy value.

***Index Terms*—High voltage transmission, HVAC, HVDC, surge impedance loading, corona, Ferranti effect, reactive compensation, loadability.**

## I. Introduction

Electric power is generated where primary energy is available and consumed where people and industry are, often hundreds of kilometers apart. High voltage (HV) transmission links the two. Because a given power can be carried at a smaller current when the voltage is higher, the $I^2R$ loss and the conductor cross-section needed fall sharply as voltage rises. This is why AC transmission voltages have progressed from 110–132 kV to 400 kV and 765 kV, and why HVDC links operate at ±500 kV and above [1]–[3].

Raising the voltage is not free. Long AC lines generate large charging currents, raise the receiving-end voltage at light load (the Ferranti effect), and are limited in loadability by voltage drop and stability rather than by the conductor [1], [8]. At the conductor surface a high electric field produces corona, which causes power loss, audible noise and radio interference [6], [9]. Reactive compensation and flexible AC transmission devices extend the reach of AC lines [4], while HVDC removes the distance limitation at the price of costly converter stations [3], [10].

This paper gives a consistent quantitative treatment of these issues using standard line theory. The contributions are: (i) line parameters, SIL and thermal ratings for 220, 400 and 765 kV overhead lines; (ii) a corona gradient assessment including the effect of conductor bundling; (iii) long-line voltage and power-transfer behavior with shunt and series compensation; (iv) loadability as a function of line length; and (v) an HVAC–HVDC cost comparison with its break-even distance and sensitivity. Section II reviews related work, Section III the theory, Sections IV–VI treat corona, compensation and HVDC, Section VII states the assumptions, Section VIII presents results and Section IX concludes.

## II. Related Work

The theory of HV transmission lines is well established [1], [2], [5], and detailed data on conductors, bundles and field effects are collected in the EPRI reference book [6]. Dunlop *et al.* derived loadability characteristics for EHV and UHV lines from thermal, voltage-drop and stability criteria [8], which remain the basis of practical line-loading guidance. Hingorani and Gyugyi describe how series and shunt compensation and power-electronic controllers extend AC transmission capability [4].

For HVDC, Arrillaga [3] and Kimbark [12] cover converter operation and system design, Bahrman and Johnson [11] explain the main technologies, and Flourentzou *et al.* [10] review voltage-source converters. Comparative studies of HVAC and HVDC [13], [14] conclude that DC becomes economic beyond a break-even distance of the order of several hundred kilometers for overhead lines, with the value depending strongly on terminal cost. This paper combines these strands in one set of calculations with transparent assumptions so that each result can be reproduced and adapted.

## III. Fundamentals of HV Transmission

Fig. 1 shows the place of the HV line in the supply chain. Power from the generating station is stepped up by the generator transformer, carried over the EHV line, and stepped down through successive substations to distribution voltage [1], [15].

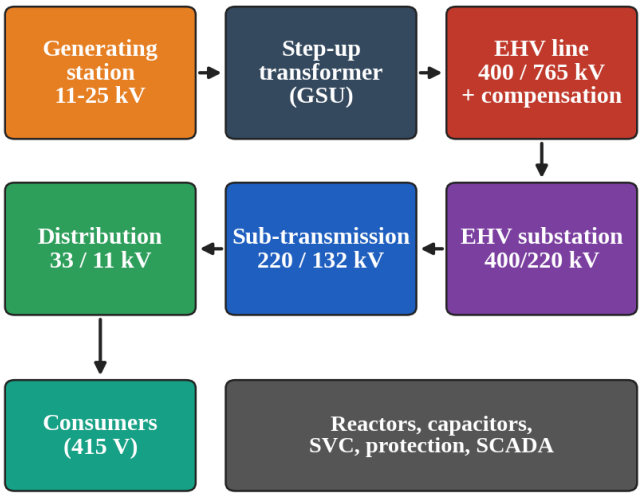



Fig. 1. Structure of an AC power system showing the voltage levels from generation to consumers.

*A. Voltage and Losses*

For a three-phase line carrying power $P$ at line voltage $V$ and power factor $\cos\varphi$, the current is $I = P/(\sqrt{3}\,V\cos\varphi)$ and the conductor loss is $3I^2Rl$. The loss as a fraction of the transmitted power is therefore

$$P_{loss} / P = PRl / (V^2\cos^2\varphi) \qquad (1)$$

where $R$ is the resistance per phase per km and $l$ the length in km. For a fixed power and conductor, loss falls with the square of voltage [2]. The thermal rating of the conductor [7] bounds the current that can be carried.

*B. Line Parameters*

For a transposed three-phase line the inductance and capacitance per phase per meter are [5]

$$L = 2\times10^{-7}\ln(D_m / D_s) \qquad (2)$$

$$C = 2\pi\varepsilon_0 / \ln(D_m / r_b) \qquad (3)$$

where $D_m$ is the geometric mean distance between phases, $D_s$ the geometric mean radius (GMR) of the phase conductor or bundle, and $r_b$ the equivalent bundle radius. Bundling $n$ subconductors raises $D_s$ and $r_b$, which lowers the reactance, raises the capacitance and reduces the surface gradient [6]. The series reactance and shunt susceptance per km are $x = 2\pi fL$ and $b = 2\pi fC$.

*C. Long-Line Model and Ferranti Effect*

For lines longer than about 250 km the distributed nature of the parameters matters. With $z = r + jx$ and $y = jb$ per km, the characteristic impedance and propagation constant are

$$Z_c = \sqrt{(z / y)}, \quad \gamma = \sqrt{(zy)} = \alpha + j\beta \qquad (4)$$

and the sending-end voltage is related to the receiving-end quantities by

$$V_S = AV_R + BI_R \qquad (5)$$

$$A = \cosh\gamma l, \quad B = Z_c\sinh\gamma l \qquad (6)$$

For a lossless line open at the receiving end, the receiving-end voltage exceeds the sending-end voltage by the factor

$$V_{R0} / V_S = 1 / \cos\beta l \qquad (7)$$

which is the Ferranti effect; it grows rapidly with length.

*D. SIL and Loadability*

The surge impedance loading is the power at which the reactive power generated by the line capacitance equals that absorbed by its inductance:

$$\text{SIL} = V^2 / Z_c \qquad (8)$$

The steady-state power-transfer limit of a lossless line with equal end voltages is

$$P_{max} = V_S V_R / (Z_c \sin\beta l) (9)$$

Following Dunlop *et al.* [8], practical loadability is the smallest of three limits: the conductor thermal limit, a 5% voltage-drop limit, and a stability limit set at 30% below $P_{max}$. The thermal limit governs short lines, the voltage-drop limit medium lines and the stability limit very long lines.

## IV. Corona and Conductor Bundling

Corona begins when the maximum surface gradient exceeds the breakdown strength of the air at the conductor. With $Q = CV_{ph}$ the charge per unit length, the average surface gradient of an $n$-conductor bundle is $E_{avg} = Q/(2\pi\varepsilon_0 nr)$ and the maximum gradient is approximately

$$E_{max} = E_{avg} 1 + (n-1)r / R_\{b\} \qquad (10)$$

where $r$ is the subconductor radius and $R_b$ the bundle radius. Peek's empirical onset gradient [9] is

$$E_o = 30m\delta(1 + 0.301 / \sqrt{(\delta r)}) \qquad (11)$$

in kV/cm peak, with $r$ in cm, air density factor δ and surface factor $m$. Here δ = 0.95 and $m$ = 0.85 are used for fair weather, and an effective $m$ = 0.6 for rain, when water drops distort the field. Onset gradients are quoted as rms values (peak divided by √2).

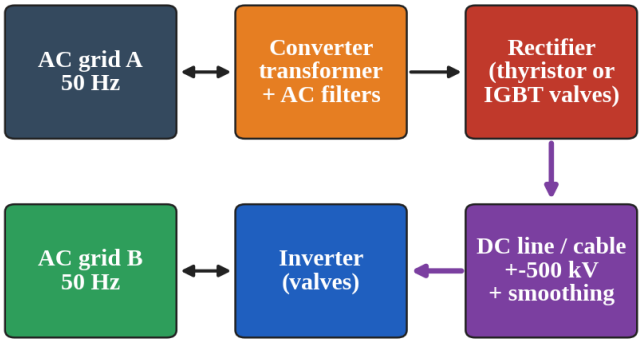
## V. Reactive Compensation and Insulation

Shunt reactors absorb the line-charging reactive power and limit the Ferranti rise; series capacitors cancel part of the line reactance and raise the power-transfer capability; and static VAR compensators and STATCOMs give fast voltage support [4]. Here compensation is idealized as uniformly distributed: a fraction $k_h$ of the shunt susceptance and a fraction $k_s$ of the series reactance are cancelled. This ignores device cost and losses, sub-synchronous resonance and the discrete placement used in practice.

Insulation must withstand lightning and switching overvoltages as well as the continuous operating voltage. At EHV levels switching surges, rather than lightning, usually set air clearances and the number of insulator units, so surge arresters and controlled (point-on-wave) breaker closing are used to limit them. Shunt reactors also help by reducing the energization overvoltage of long lines [1], [6].

## VI. HVDC Transmission

An HVDC link (Fig. 2) converts AC to DC at the sending end, carries the power on two poles, and converts it back to AC at the receiving end. Line-commutated converters (LCC) use thyristor valves, handle the largest powers and absorb reactive power from the AC system, whereas voltage-source converters (VSC) use IGBT valves, control active and reactive power independently and can supply weak or passive networks [10], [11]. Common configurations are monopolar, bipolar and back-to-back; the bipolar link continues at reduced power if one pole fails, and the back-to-back arrangement joins asynchronous grids [3], [12].




Power flow A to B shown; the link can reverse direction.

Fig. 2. Configuration of an HVDC link between two AC systems.

Because direct current has no frequency, a DC line has no steady-state charging current, no skin effect and no stability limit on distance, and it needs two conductors rather than three. The costs are the converter stations, harmonic filters and the need to clear DC faults.

## VII. Assumptions

Overhead lines use ACSR Moose conductor (31.77 mm diameter, 0.069 Ω/km at 75 °C, GMR 12.85 mm) at 50 Hz with a thermal rating of 900 A per subconductor [6], [7]. The phases are in a flat horizontal arrangement with spacings of 6.5, 11 and 14.5 m, and the bundles are single (220 kV), twin (400 kV) and quad (765 kV) with 0.457 m subconductor spacing (Table I). The geometric mean distance is 1.26 times the phase spacing. P–V curves use a load power factor of 0.95 lagging with the sending end held at 1.0 p.u.; loadability uses unity power factor. The cost model is given in Section VIII-G. All values are representative rather than specific to a utility.

TABLE I

Calculated Parameters of the HV Lines

| **Parameter** | **220 kV** | **400 kV** | **765 kV** |
|---|---|---|---|
| Bundle (Moose) | 1 × | 2 × | 4 × |
| Phase spacing (m) | 6.5 | 11 | 14.5 |
| $R$ (Ω/km, 75 °C) | 0.0690 | 0.0345 | 0.0173 |
| $X_L$ (Ω/km) | 0.406 | 0.327 | 0.282 |
| $B$ (μS/km) | 2.80 | 3.43 | 3.93 |
| $Z_c$ (Ω) | 381 | 308 | 268 |
| SIL (MW) | 127 | 519 | 2184 |
| Thermal limit (MW) | 343 | 1247 | 4770 |
| Max gradient (kV/cm rms) | 12.8 | 15.3 | 18.0 |

## VIII. Results and Discussion

*A. Voltage, Current and Loss*

Fig. 3 evaluates (1) for a 500 MW transfer at 0.95 power factor over a twin-Moose line. The I²R loss per 100 km falls from 10.97% at 132 kV to 3.95% at 220 kV, 1.19% at 400 kV and 0.33% at 765 kV, a twelve-fold reduction between 220 and 765 kV, in line with the (765/220)² ratio. The current at 132 kV, 2302 A, exceeds the 1800 A thermal limit of the conductor, so low voltages are not merely lossy but infeasible for this power.

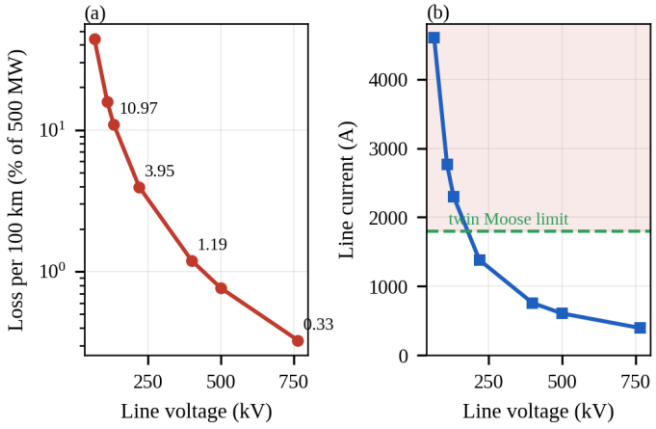



Fig. 3. (a) I²R loss per 100 km and (b) line current versus voltage for a 500 MW transfer with a twin-Moose line.

*B. Line Parameters and SIL*

Table I shows that bundling and higher voltage reduce the characteristic impedance from 381 Ω to 268 Ω. Because SIL varies as $V^2/Z_c$, it rises from 127 MW at 220 kV to 519 MW at 400 kV and 2184 MW at 765 kV, a seventeen-fold increase for a 3.5-fold increase in voltage. The thermal limit exceeds SIL by a factor of 2.4 at 400 kV and 2.2 at 765 kV, which is why short lines can be loaded well above SIL.

*C. Corona*

In Fig. 4(a) the maximum gradient is 12.8 kV/cm at 220 kV, 15.3 kV/cm at 400 kV and 18.0 kV/cm at 765 kV. All are below the fair-weather onset of 21.3 kV/cm, but the 400 and 765 kV lines exceed the rain onset of 15.1 kV/cm, so corona activity is expected in wet weather and the bundle must be designed for it. Fig. 4(b) shows the effect of bundling at 765 kV: a single conductor reaches 39.5 kV/cm, four conductors 18.0 kV/cm, and six conductors 13.8 kV/cm, which falls below the rain onset.

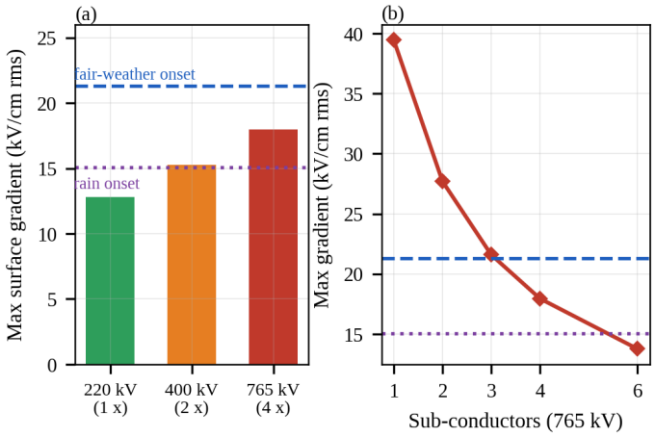



Fig. 4. (a) Maximum surface gradient at three voltage levels and (b) effect of the number of subconductors at 765 kV, against fair-weather and rain onset gradients.

*D. Voltage Behavior and Compensation*

Fig. 5(a) shows the no-load voltage rise of a 400 kV line. At 300 km it is 5.3%, above the usual 5% limit; 50% shunt compensation reduces it to 2.6% and 80% to 1.0%. In Fig. 5(b) the P–V curve of the 300 km line at 0.95 power factor reaches its nose at 584 MW (0.62 p.u.), only 1.1 times SIL, so voltage collapse is the practical limit. Shunt reactors alone do not help here (nose 565 MW) because they remove the line's reactive support at load, whereas 40% series compensation raises the nose to 899 MW, an increase of 54%. Combined compensation gives 882 MW; because reactors lower the nose slightly, they are best switched in at light load.

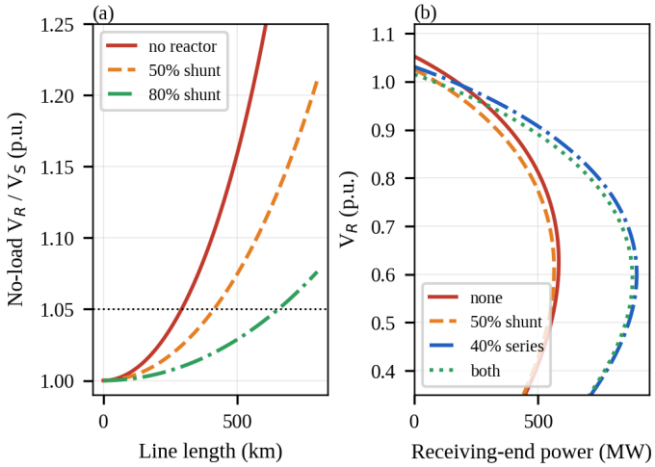



Fig. 5. (a) No-load voltage rise of a 400 kV line and (b) P–V curves of a 300 km, 400 kV line with shunt and series compensation.

*E. Reactive Power, Voltage Profile and Angle*

Line charging grows with the square of voltage and linearly with length. Fig. 6(a) shows that a 400 km line generates about 220 Mvar at 400 kV and 921 Mvar at 765 kV, which must be absorbed by reactors or by the sending-end source at light load. Fig. 6(b) shows the voltage profile of a 400 km, 400 kV line with the receiving end held at 1.0 p.u. At 0.5 SIL the voltage is above the receiving-end value along most of the line, with the sending end 4.3% lower; at 1.0 SIL the profile is nearly flat apart from a resistive drop of about 4% over the line; and at 1.5 SIL the sending-end voltage must be about 16% higher, which is not acceptable without compensation.

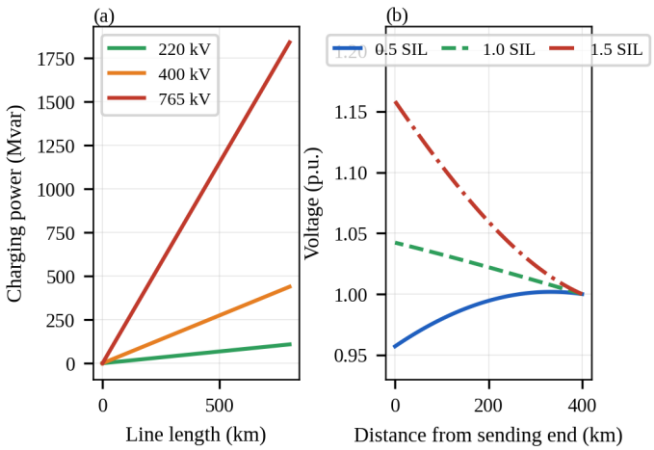



Fig. 6. (a) Line-charging reactive power versus length and (b) voltage profile of a 400 km, 400 kV line at 0.5, 1.0 and 1.5 SIL.

Fig. 7 plots (9) for the 400 kV line. Carrying SIL requires an angle of βl between the end voltages, about 12° at 200 km, 24° at 400 km and 36° at 600 km, so long lines operate closer to their stability limit. The maximum power falls from 2468 MW at 200 km to 1262 MW at 400 km and 874 MW at 600 km. The dots mark the 30% margin points used in the loadability limit.

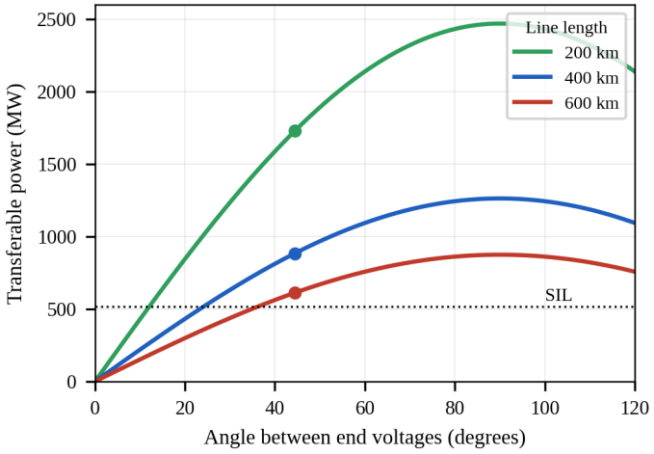



Fig. 7. Power–angle curves of a lossless 400 kV line for three lengths; dots mark 70% of maximum power.

*F. Loadability versus Length*

Fig. 8 gives loadability in multiples of SIL. The 400 kV line is thermally limited at 2.4 SIL up to about 90 km, after which the 5% voltage-drop limit governs: 1.42 SIL at 170 km, 1.04 SIL at 300 km and 0.89 SIL at 600 km. The 765 kV line follows the same pattern, with the transition at about 120 km and 1.15 SIL at 300 km. The 30% stability limit does not bind within 800 km in this strong-source model; source impedances would lower it in practice. These results agree in shape with the classical loadability curve of [8].

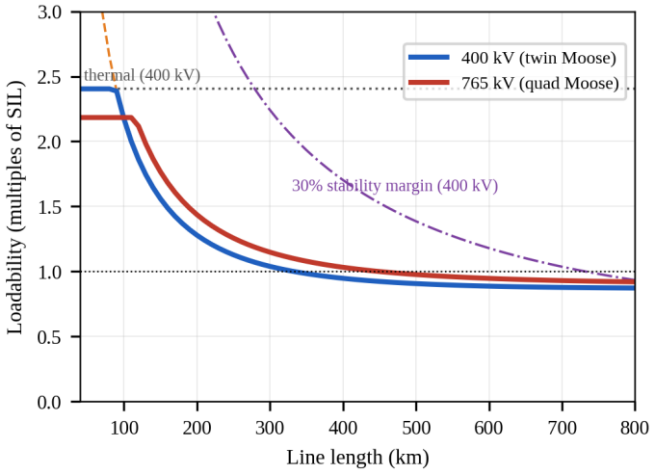



Fig. 8. Line loadability in multiples of SIL versus length for 400 and 765 kV lines, with the three limits shown for 400 kV.

Table IV converts these limits to megawatts and can be used as a first screening guide for voltage class. A 220 kV line is limited to about 230 MW at 100 km and 115 MW at 300 km, whereas a 400 kV line carries 539 MW at 300 km and a 765 kV line 2509 MW.

TABLE IV

Loadability in MW from the Calculated Limits

| **Line** | **100 km** | **300 km** | **600 km** |
|---|---|---|---|
| 220 kV | 230 | 115 | 103 |
| 400 kV | 1128 | 539 | 460 |
| 765 kV | 4770 | 2509 | 2069 |

*G. HVAC versus HVDC Cost*

The comparison is for 1000 MW. HVAC uses one 765 kV circuit (0.33% I²R loss per 100 km) and HVDC a ±500 kV bipole (0.256% per 100 km plus 1.5% in the converters). Cost is the present value of capital and losses:

$$C(l) = 2T + cl + K\eta(l) \quad (12)$$

where $T$ is the terminal cost per end, $c$ the line cost per km (AC adds 0.10 USD million/km of compensation beyond 300 km), $\eta(l)$ the loss in percent and $K$ the present value of 1% loss,

$$K = P \cdot 8760 \cdot \mathrm{LF} \cdot p_e \cdot \mathrm{AF} / 100 \quad (13)$$

with load factor LF = 0.8, energy value $p_e$ = 60 USD/MWh and annuity factor $\mathrm{AF} = (1 - (1+i)^{-N})/i = 10.67$ for $i$ = 8% and $N$ = 25 years, giving $K$ = 44.9 USD million per percent. The break-even distance satisfies $C_{AC}(l_{be}) = C_{DC}(l_{be})$. The assumed costs (Table II) lie within ranges reported in the literature [13], [14] but are illustrative.

TABLE II

Comparison of HVAC and HVDC (1000 MW)

| **Aspect** | **HVAC 765 kV** | **HVDC ±500 kV** |
|---|---|---|
| Reactive power | Line charging; reactors, SVC | None on line; LCC needs support |
| Distance limit | Voltage and stability | No stability limit |
| Interconnection | Synchronous only | Asynchronous possible |
| Power control | Angle and voltage | Direct, fast |
| Line conductors | 3 per circuit | 2 (bipole) |
| Line cost (USD M/km) | 1.00 | 0.70 |
| Terminal cost (USD M/end) | 30 | 140 |
| I²R loss, 1000 km | 3.3% | 2.6% + 1.5% converters |

In Fig. 9 the curves cross at 740 km. Below this HVAC is cheaper because its terminals cost less; above it HVDC wins because its line is cheaper and needs no compensation. Table III shows that at 500 km HVAC saves about 101 USD million, while at 1000 km HVDC saves 114 and at 1500 km 330 USD million. Note that in this model the HVDC loss at 1000 km (4.1%) exceeds the I²R loss of the AC line (3.3%), which excludes compensation equipment losses; the economic gain of HVDC comes mainly from line and compensation cost, not from loss.

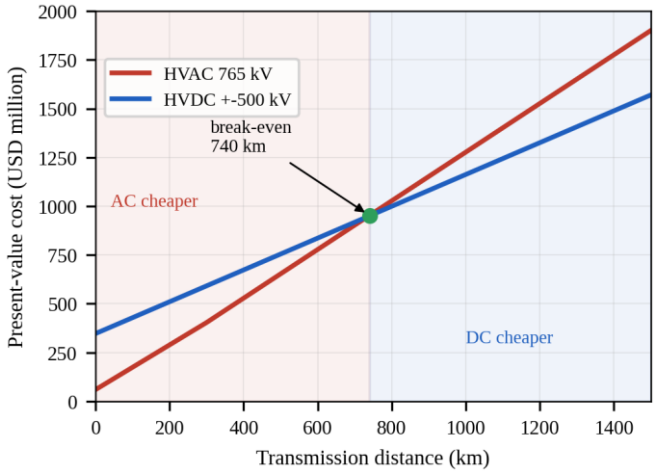



Fig. 9. Present-value cost of HVAC and HVDC versus transmission distance for 1000 MW.

TABLE III

Present-Value Cost (USD Million)

| Distance (km) | HVAC | HVDC | Cheaper |
|---|---|---|---|
| 300 | 404 | 592 | HVAC |
| 500 | 653 | 755 | HVAC |
| 740 | 952 | 950 | equal |
| 1000 | 1277 | 1162 | HVDC |
| 1500 | 1900 | 1570 | HVDC |

Fig. 10 shows the sensitivity of the break-even distance. It rises almost linearly with converter-station cost, from 550 km at USD 100 million per end to 1015 km at USD 200 million per end for an energy value of USD 60/MWh. A higher energy value shortens the break-even slightly because the AC loss penalty grows with distance faster than the DC one. Over all cases the break-even lies between 515 and 1040 km, so the choice for a specific corridor needs a project-specific estimate.

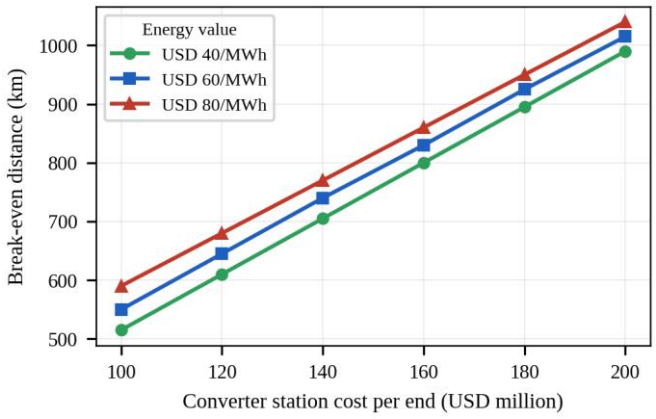



Fig. 10. Break-even distance versus converter-station cost for three energy values.

## IX. Conclusion

This paper analyzed HV overhead transmission using standard line theory and a transparent cost model. Raising the voltage from 220 to 765 kV reduces $I^2R$ loss twelve-fold for a given power and raises SIL from 127 to 2184 MW. Corona gradients of the 400 and 765 kV bundles exceed the rain onset, so bundle design must consider wet weather. A 300 km, 400 kV line shows a 5.3% Ferranti rise and a P–V nose of only 584 MW; shunt reactors tame the rise, but series compensation is what raises transfer capability (to 899 MW). Loadability falls from the thermal limit at short lengths to about 1.0 SIL at

300 km. For 1000 MW, HVDC becomes the cheaper option beyond about 740 km under the stated assumptions, with a broad range of 515–1040 km. The results rest on representative conductor, geometry and cost data, a lossless-source idealization and uniformly distributed compensation, so a specific project needs detailed load-flow, stability and cost studies. Future work can add transient and sub-synchronous resonance analysis, VSC-HVDC and multi-terminal grids, and measured corona data.

**Acknowledgment**

The author thanks [guide's name] and the Department of Electrical Engineering, [name of institute], for guidance and support.

**References**

[1] P. Kundur, *Power System Stability and Control*. New York, NY, USA: McGraw-Hill, 1994.

[2] J. D. Glover, M. S. Sarma, and T. J. Overbye, *Power System Analysis and Design*, 6th ed. Boston, MA, USA: Cengage Learning, 2017.

[3] J. Arrillaga, *High Voltage Direct Current Transmission*, 2nd ed. London, U.K.: Institution of Electrical Engineers, 1998.

[4] N. G. Hingorani and L. Gyugyi, *Understanding FACTS: Concepts and Technology of Flexible AC Transmission Systems*. New York, NY, USA: IEEE Press, 2000.

[5] J. J. Grainger and W. D. Stevenson, *Power System Analysis*. New York, NY, USA: McGraw-Hill, 1994.

[6] Electric Power Research Institute, *EPRI AC Transmission Line Reference Book—200 kV and Above*, 3rd ed. Palo Alto, CA, USA: EPRI, 2005.

[7] *IEEE Standard for Calculating the Current-Temperature Relationship of Bare Overhead Conductors*, IEEE Std 738-2012, 2013.

[8] R. D. Dunlop, R. Gutman, and P. P. Marchenko, "Analytical development of loadability characteristics for EHV and UHV transmission lines," *IEEE Trans. Power App. Syst.*, vol. PAS-98, no. 2, pp. 606–617, Mar. 1979.

[9] F. W. Peek, *Dielectric Phenomena in High Voltage Engineering*, 3rd ed. New York, NY, USA: McGraw-Hill, 1929.

[10] G. Flourentzou, V. G. Agelidis, and G. D. Demetriades, "VSC-based HVDC power transmission systems: An overview," *IEEE Trans. Power Electron.*, vol. 24, no. 3, pp. 592–602, Mar. 2009.

[11] D. Bahrman and B. K. Johnson, "The ABCs of HVDC transmission technologies," *IEEE Power Energy Mag.*, vol. 5, no. 2, pp. 32–44, Mar./Apr. 2007.

[12] E. W. Kimbark, *Direct Current Transmission*, vol. 1. New York, NY, USA: Wiley, 1971.

[13] N. Kalair, N. Abas, and N. Khan, "Comparative study of HVAC and HVDC transmission systems," *Renew. Sustain. Energy Rev.*, vol. 59, pp. 1653–1675, Jun. 2016.

[14] R. Rudervall, J. P. Charpentier, and R. Sharma, "High voltage direct current (HVDC) transmission systems technology review paper," presented at Energy Week 2000, World Bank, Washington, DC, USA, Mar. 2000.

[15] L. L. Grigsby, Ed., *Electric Power Generation, Transmission, and Distribution*, 3rd ed. Boca Raton, FL, USA: CRC Press, 2012.